

A Flexible Microporous Hydrogen-Bonded Organic Framework for Gas Sorption and Separation

Hailong Wang,[†] Bin Li,[†] Hui Wu,[‡] Tong-Liang Hu,[†] Zizhu Yao,[§] Wei Zhou,^{*,‡} Shengchang Xiang,[§] and Banglin Chen^{*,†}

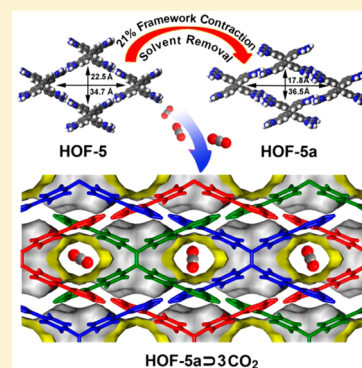
[†]Department of Chemistry, University of Texas at San Antonio, San Antonio, Texas 78249-0698, United States

[‡]NIST Center for Neutron Research, National Institute of Standards & Technology, Gaithersburg, Maryland 20899-6102, United States

[§]College of Material Science and Engineering, Fujian Provincial Key Laboratory of Polymer Materials, Fujian Normal University, 32 Shangsang Road, Fuzhou 350007, China

S Supporting Information

ABSTRACT: A microporous three-dimensional hydrogen-bonded organic framework (HOF-5) has been constructed from a new organic linker 4,4',4'',4'''-tetra(2,4-diamino-1,3,5-triazin-6-yl)tetraphenylethene. Activated HOF-5a exhibits a stepwise N₂ adsorption isotherm at 77 K, suggesting framework flexibility. The structure of activated HOF-5a has been established by powder X-ray diffraction studies, indicating a significant framework contraction from as-synthesized HOF-5 to activated HOF-5a of ~21% by volume. HOF-5a shows moderately high porosity with a Brunauer–Emmett–Teller (BET) surface area of 1101 m²/g, and takes up a large amount of acetylene and carbon dioxide under ambient conditions. Powder neutron diffraction studies and theoretical calculations reveal that suitable pore sizes, curvatures, and functional sites collectively enable HOF-5a to encapsulate a high density of carbon dioxide molecules packed in a pseudo-one-dimensional array along the pore channel.



INTRODUCTION

Over the years, research on porous media, from traditional zeolites, carbons, and mesoporous materials to metal–organic frameworks (MOFs) and covalent-organic frameworks (COFs), has demonstrated the crucial roles of such materials for the advancement of science and technology.^{1–5} The extensive pursuit of MOFs and COFs over the past two decades has not only led to new porous materials that can mimic traditional zeolites and porous carbons, but has also generated a number of novel materials with superior properties, thus rendering them promising for gas storage/separation, sensing, heterogeneous catalysis, and biomedical applications.^{3–5}

Compared with MOFs and COFs, which are self-assembled through coordination and covalent bonding of their corresponding building units, the hydrogen-bonded organic frameworks (HOFs), self-assembled frameworks through weaker hydrogen bonding interactions among molecular organic linkers, are much more fragile and difficult to stabilize.^{6,7} It is therefore not surprising that research on HOFs has been significantly lagging behind that of MOFs and COFs, although the concepts to construct MOFs and HOFs were basically proposed during the same period around the early 1990s.

Recently, there has been a renewed interest in the exploration of porous HOFs.^{8,9} This is because HOFs can be easily synthesized and characterized. Furthermore, the more straightforward processing and facile recycling (simply through

recrystallization) have enabled them to be particularly useful for device implementation.¹⁰ Some progress has been made to stabilize HOFs and thus to establish permanent porosities. Until now, a dozen HOFs have been discovered to display permanent porosities as confirmed by vapor/gas sorption isotherms.^{8,9} A few of them even exhibit properties superior to other porous materials for the separation of C₂H₂/C₂H₄,^{9a} C₂H₂/CO₂,^{9b} and fluororocarbons^{8f} as well as chiral secondary alcohols,^{9c} exemplifying the bright promise of HOFs as a new category of functional materials.

Although research on HOFs has been developed for quite a long time, those with both established permanent porosities by gas sorption isotherms and functional properties are still rare. Some in-depth systematical studies, including the exploration of new hydrogen bonding motifs, backbones, and organic linkers for the construction of HOFs and detailed crystallographic studies on framework robustness and flexibility, are certainly necessary before we can harness the rich chemistry of HOFs to rationally design and synthesize porous functional materials. By incorporating the well-known hydrogen bonding motif DAT (2,4-diaminotriazinyl group) with the tetraphenylethylene (TPE) backbone, we developed a new organic linker (L) (see Figure 1a) for the assembly of a novel HOF, which we named “HOF-5”. Herein, we report the crystal structure of as-

Received: June 1, 2015

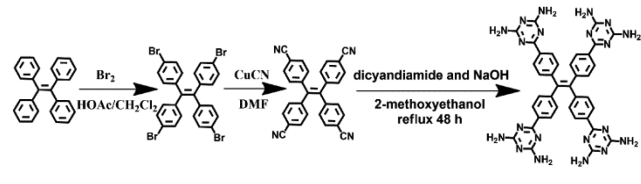
Published: July 27, 2015

synthesized HOF-5, showing its microporous nature. HOF-5 framework was found to be quite flexible. Upon activation, the structure contracts significantly with a change in crystal symmetry, as revealed by powder X-ray diffraction studies. The resulting fully activated HOF-5a has a moderately high Brunauer–Emmett–Teller (BET) surface area of 1101 m²/g, and exhibits quite interesting gas sorption behaviors, particularly for CO₂ capture and separation (CCS). The CO₂ uptake is ~90 cm³/g (86 cm³/cm³) at 1 atm and 296 K, which is the highest value among all porous HOFs, and comparable to those very few MOFs and COFs exhibiting high performance for postcombustion CCS. The specific binding of HOF-5a for CO₂ molecules has been further established by neutron powder diffraction studies and density-functional theory (DFT) calculations.

EXPERIMENTAL SECTION

General Remarks. All reagents and solvents were used directly as received from the chemical supplier without further purification. The precursors, tetra(4-bromophenyl)ethylene and tetra(4-cyanophenyl)ethylene, were prepared according to a slight modification of the reported procedures (Scheme 1).^{11,12} During the preparation of this

Scheme 1. Schematic Synthesis of the Organic Linker L for the Self-Assembly of HOF-5



manuscript, this organic ligand was reported to assemble a nonporous hydrogen-bonded organic framework,¹³ so the detailed synthesis of the organic ligand was provided in the Supporting Information.

IAST Calculation. Adsorption isotherms and gas selectivities of mixed C₂H₂/CH₄ (50:50), CO₂/CH₄ (50:50), and CO₂/N₂ (10:90) at different temperatures were calculated based on the ideal adsorbed solution theory (IAST) proposed by Myers and Prausnitz.¹⁴ In order to predict the sorption performance of this HOF toward the separation of binary mixed gases, the parameters fitted from the single-component C₂H₂, CO₂, CH₄, and N₂ adsorption isotherms based on the dual-site Langmuir–Freundlich (DSLFF) model were used in the IAST calculations.¹⁵ The fitting parameters of the DSLFF equation are listed in Table S1.

Single Crystal and Powder X-ray Crystallography. Crystallographic data of an as-synthesized HOF-5 single crystal were collected on an Oxford Diffraction SuperNova diffractometer with Cu K α radiation ($\lambda = 1.54184$ Å) at 100.00(16) K. Final unit cell parameters were derived from the global refinements of reflections obtained from the integration of all frame data. The collected frames were integrated using the preliminary cell-orientation matrix. CrysAlisPro Agilent Technologies software was used for collecting the frames of data, indexing the reflections, and determining the lattice constants, and SCALE3 ABSPACK software was utilized for the absorption correction. The structure was solved using the direct method (SHELXS-97) and refined utilizing full-matrix least-squares (SHELXL-97) on F^2 .¹⁶ Anisotropic thermal parameters were used for the nonhydrogen atoms and isotropic parameters for the hydrogen atoms. Hydrogen atoms were added geometrically and refined using a riding model. In addition, we note that the “SQUEEZE” command was employed because of the seriously disordered THF, DMF, and DMSO molecules in the HOF pores.

Powder X-ray diffraction (powder XRD) measurements were conducted on as-synthesized HOF-5 crystals in mother liquid, fully activated HOF-5a, and acetone regenerated HOF-5a, all sealed in glass

capillaries, using a Rigaku Ultima IV diffractometer with Cu K α radiation. The powder XRD pattern of activated HOF-5a sample can be indexed using a monoclinic system, and the space group was identified as $C2/m$. The structure was then solved using the direct method. Finally, Rietveld refinement was performed on the powder XRD pattern using the GSAS package.¹⁸ Refinement on the lattice parameters, background, and peak profile, as well as the atomic positions of C and N with constraints applied on C–C and C–N bond lengths yielded the agreement factors of $R_{wp} = 0.0625$ and $R_p = 0.0488$, which strongly confirms the validity of our structure solution. The positions of H atoms were estimated from the geometry and the common length of C–H bonds of the benzene ring and N–H bonds of the primary amine. Selected crystallographic data and pertinent information for these two phases are summarized in Table 1. CCDC

Table 1. Crystallographic and Refinement Parameters for HOF-5 and HOF-5a

crystal data	HOF-5	HOF-5a
system	monoclinic	monoclinic
space group	$C2/c$	$C2/m$
MF	C ₃₈ H ₃₂ N ₂₀	C ₃₈ H ₃₂ N ₂₀
FW	768.84	768.84
$a/\text{Å}$	21.6470(5)	14.3476(19)
$b/\text{Å}$	22.0832(5)	17.8692(21)
$c/\text{Å}$	14.1759(3)	12.2628(20)
$\alpha/^\circ$	90	90
$\beta/^\circ$	92.692(2)	121.697(9)
$\gamma/^\circ$	90	90
volume/Å ³	6769.1(3)	2675.0(7)
Z	4	2
density/g/cm ³	0.754	0.955
solvent-accessible void space/%	55.3	41.1
theoretical pore volume/cm ³ /g	0.72 ^a	0.43 ^a
refinement parameters	$R_1 = 0.0585^b$ $wR_2 = 0.1769^c$	$R_{wp} = 0.0625$ $R_p = 0.0488$

^aCalculated on the basis of the HOF crystal structures using PLATON software.¹⁷ ^b $R_1 = \sum |F_0 - |F_c|| / \sum |F_0|$. ^c $wR_2 = [\sum w(F_0^2 - F_c^2)^2 / \sum w(F_0^2)^2]^{1/2}$.

1057513 and 1052041 for HOF-5 and HOF-5a, respectively, contain the supplementary crystallographic data for this paper. These data can be obtained free of charge from the Cambridge Crystallographic Data Centre via www.ccdc.cam.ac.uk/data_request/cif.

Neutron Diffraction Experiment. Powder neutron diffraction data were collected using the BT-1 neutron powder diffractometer at the National Institute of Standards and Technology (NIST) Center for Neutron Research. A Ge(311) monochromator with a 75° takeoff angle, $\lambda = 2.0787(2)$ Å, and in-pile collimation of 60 min of arc was used. Data were collected over the range of 1.3–166.3° (2θ) with a step size of 0.05°. Fully activated HOF-5a sample was loaded in a vanadium can equipped with a capillary gas line and a packless valve. A closed-cycle He refrigerator was used for sample temperature control. The sample of activated HOF-5a was measured first at the temperatures of 6, 100, and 200 K. No phase transition was observed, indicating a relatively “robust” HOF-5a pore structure within this temperature range. To probe the preferential CO₂ adsorption locations, a predetermined amount of CO₂ (~1.5CO₂ per L molecule) was loaded into the sample at room temperature. The sample was then slowly cooled to 200 K before diffraction data were collected.

Rietveld structural refinement was also performed on the neutron diffraction data.¹⁸ Due to the large incoherent background (mainly from the elemental H in HOF-5a), the overall data quality is modest, and thus both the HOF-5 building block (L) and CO₂ molecules were treated as rigid bodies in Rietveld refinement (to limit the number of variables), with the molecule orientation and center of mass freely

refined. Final refinement on the positions/orientations of the rigid bodies, thermal factors, occupancies, lattice parameters, background, and profiles converges with satisfactory *R*-factors.

Density-Functional Theory Calculations. First-principles density-functional theory (DFT) calculations were performed using the Quantum-Espresso package.¹⁹ A semiempirical addition of dispersive forces to conventional DFT was included in the calculation to account for van der Waals interactions.²⁰ We used Vanderbilt-type ultrasoft pseudopotentials and generalized gradient approximation (GGA) with Perdew–Burke–Ernzerhof (PBE) exchange correlation. A cutoff energy of 544 eV and a $2 \times 2 \times 2$ *k*-point mesh (generated using the Monkhorst-Pack scheme) were found to be enough for the total energy to converge within 0.01 meV/atom. We first optimized the HOF-5a structure. The CO₂ gas molecule was then introduced to the optimized HOF structure at the experimentally identified adsorption site, followed by a full structural relaxation. To obtain the gas binding energy, a CO₂ gas molecule placed in a supercell with the same cell dimensions was also relaxed as a reference. The static binding energy (at *T* = 0 K) was then calculated using $E_B = E(\text{HOF-5a}) + E(\text{CO}_2) - E(\text{HOF-5a} \supset \text{CO}_2)$.

RESULTS AND DISCUSSION

Self-Assembly of HOF-5. The bromination reaction between tetraphenylethylene (TPE) and Br₂ in a mixed glacial acetic acid/dichloromethane solution yields tetra(4-bromophenyl)ethylene. Reaction time of 30 min is optimized on the basis of TLC detection (a longer reaction time led to the formation of unknown impurities). The corresponding organic linker L is obtained by the reaction of tetra(4-cyanophenyl)ethylene with dicyandiamide in the presence of NaOH. HOF-5, as pale yellowish block-shaped single crystals, is self-assembled from organic linker L, through the slow diffusion of tetrahydrofuran (THF) into a DMF/DMSO (2:1) solution containing L at room temperature.

Crystal Structure of HOF-5. The single-crystal X-ray diffraction analysis at 100 K reveals that as-synthesized HOF-5 crystallizes in the monoclinic system and *C2/c* space group, and exhibits a microporous three-dimensional (3D) hydrogen-bonded structure. In the crystal structure of HOF-5, each organic linker is connected with eight neighboring organic linkers via 20 N–H···N hydrogen bonds between the 2,4-diaminotriazinyl (DAT) motifs. A two-dimensional (2D) supramolecular grid is achieved through the hydrogen bonds N4–H4A···N7#1 and N9–H9A···N2#4 (symmetry code #1: $1.5 - x + 3/2, 0.5 + y, 1.5 - z$ and #4: $1.5 - x, -0.5 + y, 1.5 - z$), as shown in Figure S1. The hydrogen-bonded adjacent sheets are stacked in a repeated –[A–B–C]– staggered configuration through additional hydrogen bonding interactions to form the three-dimensional HOF-5. Topologically, we can consider the building linker L as a four-connected node and the center of neighboring six DAT motifs as a six-connected node to assemble into a hydrogen bonded organic framework net of a binodal (4,6)-connected topology with the Schläfli symbol of $\{3^2.4^4.5^4.6^4.7\}2\{3^2.6^2.7^2\}$ (Figure 1a–c). It contains two-dimensional irregular channels with pore sizes in the range of 3.7 Å to 6.8 Å, as demonstrated by the PLATON software analysis. The open channels are shown in Figure 1d and 1e, with the window sizes of $\sim 4.0 \times 6.8$ Å along the $[\bar{1}01]$ direction and $\sim 3.9 \times 5.4$ and 4.1×6.8 Å along the $[001]$ direction.

The purity of the bulk HOF-5 sample was confirmed by ¹H NMR spectroscopy, thermogravimetric analysis (TGA), and powder XRD studies. ¹H and ¹³C NMR spectra of as-synthesized HOF-5 crystals in DMSO-*d*₆ solution indicate that HOF-5 contains the pure organic linker and DMF, DMSO,

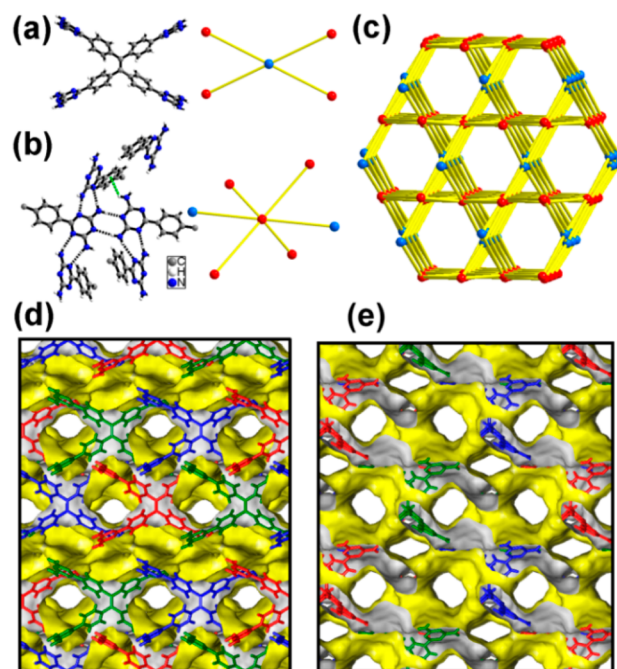


Figure 1. Crystal structure of HOF-5 showing (a) the organic building block acting as a 4-connected node (cyan ball); (b) six neighboring DATs connected through the hydrogen bonding and weak van der Waals interactions [the center acting as a 6-connected node (red ball)]; (c) a binodal (4,6)-connected net; (d and e) packing diagram of HOF-5 along the $[\bar{1}01]$ and $[001]$ direction, respectively, showing the pore surfaces of 2D channels highlighted as yellow/gray (inner/outer) curved planes with pore sizes of (d) $\sim 4.0 \times 6.8$ Å and (e) $\sim 3.9 \times 5.4$ and 4.1×6.8 Å.

and THF molecules (Figure S2). The TGA curve of HOF-5 (Figure S3) shows that the THF, DMF, and DMSO molecules are gradually lost starting from room temperature to 230 °C. The powder XRD pattern of as-synthesized HOF-5 (immersed in its mother liquid) at room temperature matches well with the simulated XRD pattern based on the crystal structure (without considering solvent molecules), in terms of the peak positions, confirming that the powder sample is a single-phase (Figure S4).

Crystal Structure of HOF-5a. Before the gas sorption measurement, the acetone-exchanged crystals of HOF-5 were activated in high vacuum at room temperature to generate activated HOF-5a. During the transition, it was found that the pale-yellowish single crystals of HOF-5 were changed into a light yellow crystalline material, HOF-5a (Figure S5). The flexible nature of HOF-5 is indicated by powder XRD patterns of HOF-5 and HOF-5a (Figure S6), which motivated us to further investigate the structure of activated HOF-5a and their framework transformation during the activation. The structure of HOF-5a was solved using the direct method, and Rietveld refinement was performed on the powder XRD data (see Figure S7). Activated HOF-5a crystallizes in space group *C2/m*. Each organic linker in HOF-5a is still linked by eight organic linkers but via 24 hydrogen bonds between DATs (20 hydrogen bonds in HOF-5). The hydrogen bonding interactions in HOF-5a are apparently strengthened, as demonstrated in the shorter D···A distances and angles of D–H···A much closer to 180° (Table 2), which stabilizes the activated framework. HOF-5a retains the same framework connectivity and topology of HOF-5 as a binodal (4,6)-

Table 2. Comparison of the Hydrogen Bonding Interactions and Close Contact in the Crystal Structures of HOF-5 and HOF-5a

D–H...A	distance of D...A (Å)	angle of D–H...A (deg)
HOF-5		
N4–H4A...N7#1	2.924(4)	175.8
N4–H4B...N6#2	2.986(4)	176.3
N5–H5B...N3#3	3.030(5)	153.8
N9–H9A...N2#4	3.193(4)	166.8
N9–H9B...N1#2	3.385(4)	160.5
N10–H10B...N8#3 ^a	5.394(2)	152.6
HOF-5a		
N19–H16...N22#1	2.966(5)	173.2
N19–H17...N20#2	3.011(1)	175.7
N18–H15...N21#3	2.920(8)	170.6
N19–H16...N22#1	2.966(5)	173.2
N19–H17...N20#2	3.011(1)	175.7
N18–H15...N21#3	2.920(8)	170.6

^aClose contact among DATs for HOF-5. Symmetric code for HOF-5, #1: 1.5 – x, 0.5 + y, 1.5 – z, #2: 1.5 – x, 1.5 – y, 1 – z, #3: 1 – x, y, 1.5 – z, #4: 1.5 – x, –0.5 + y, 1.5 – z. For HOF-5a, #1: 1.5 – x, 0.5 – y, 1 – z, #2: 1 – x, y, 1 – z, #3: 1 – x, y, –z.

connected net with the Schläfli symbol of $\{3^2.4^4.5^4.6^4.7\}2-\{3^2.6^2.7^2\}$ (Figure 2a and 2b).

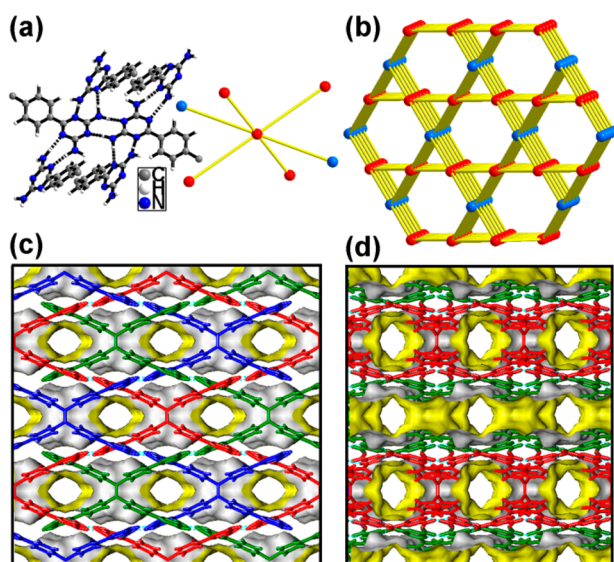


Figure 2. Crystal structure of HOF-5a indicating (a) multiple hydrogen bonding interactions between neighboring six DAT groups [their center acting as a 6-connected node (red balls), while the center of each organic linker acting as a 4-connected node (cyan ball)]; (b) a binodal (4,6)-connected hydrogen-bonded organic framework net; (c and d) packing diagram along the [001] and [100] directions, respectively, showing the pore surfaces of 2D channels highlighted as yellow/gray (inner/outer) curved planes with pore sizes of (c) $\sim 3.9 \times 6.8$ Å and (d) $\sim 3.9 \times 5.5$ Å.

The framework quite significantly contracts after solvent removal. As shown in Table 1, the unit cell volume changes from 6769.1 Å³ ($Z = 4$) in HOF-5 to 2675.0 Å³ ($Z = 2$) in HOF-5a with $\sim 21\%$ framework contraction. Accordingly, HOF-5a has less solvent-accessible void space (41.1%) than that for HOF-5 (55.3%). More specifically, the supramolecular grid of $\sim 22.5 \times 34.7$ Å in HOF-5 contracts to $\sim 17.8 \times 36.5$ Å

in HOF-5a (Figure S1). The neighboring layers slip slightly with respect to each other as well (Figure S8). The 2D pore channels in HOF-5a are more ordered and slightly smaller than those in HOF-5. They are $\sim 3.9 \times 6.8$ Å along the [001] direction (Figure 2c) and $\sim 3.9 \times 5.5$ Å along the [100] direction (Figure 2d). We point out that, in comparison with other HOFs containing DAT moieties (which usually collapses after removal of guests), all amino groups of HOF-5a utilized to support the hydrogen-bonded organic channels should be responsible for the permanent porosity. In addition, HOF-5 can be basically recovered from HOF-5a by immersing it into dry acetone, as indicated by the powder XRD patterns (Figure S9). Then the acetone-regenerated sample can be subsequently activated again to reproduce HOF-5a. We repeated the cycling process three times, and the powder XRD patterns of HOF-5a remain nearly unchanged (Figure S9), suggesting good reversibility between HOF-5 and HOF-5a.

Establishment of Permanent Porosity. The porous nature of HOF-5a, as revealed by its crystal structure, encouraged us to examine its permanent porosity through the gas sorption studies. HOF-5a displays stepwise N₂ adsorption and desorption isotherms at 77 K, with a narrow hysteresis loop (Figure 3). Such stepwise N₂ gas sorption isotherms have been

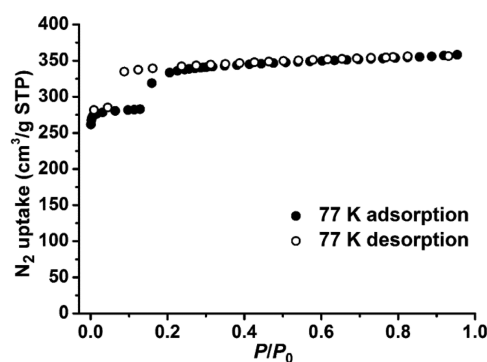


Figure 3. N₂ adsorption/desorption isotherms of HOF-5a.

found in many well-known flexible MOFs, but have not been previously observed in porous HOFs. The unique sorption behaviors indicate that HOF-5a exhibits a flexible robust (porous) framework. The BET surface area of HOF-5a derived from the N₂ isotherm is 1101 m²/g (Figure S10). The experimental pore volume of HOF-5a is 0.44 cm³/g, corresponding to the first step N₂ adsorption isotherm at 77 K, recorded at $P/P_0 = 0.13$. This value matches well with the calculated value of 0.43 cm³/g for HOF-5a deduced from the crystal structure. In addition, the total pore volume is 0.55 cm³/g based on the N₂ uptake at $P/P_0 = 0.96$, which is lower than the theoretical pore volume (0.72 cm³/g) from the crystal structure of HOF-5 (without considering the solvent molecules), suggesting that HOF-5a has not been fully expanded back to HOF-5 under this sorption condition.

Gas Sorption. Single-component gas sorption isotherms recorded on HOF-5a at two different temperatures are presented in Figure 4a and 4b. The adsorption isotherm for C₂H₂ measured at 296 K shows that HOF-5a adsorbs a relatively high amount of C₂H₂ with an uptake of 101.7 cm³/g (STP) at 1 atm. This is the highest C₂H₂ uptake among all reported HOFs (Table 3). At 273 K, a stepwise adsorption isotherm of C₂H₂ is observed as well because of the framework flexibility. Its C₂H₂ uptake at 1 atm is 182.0 cm³/g (173.8 cm³/

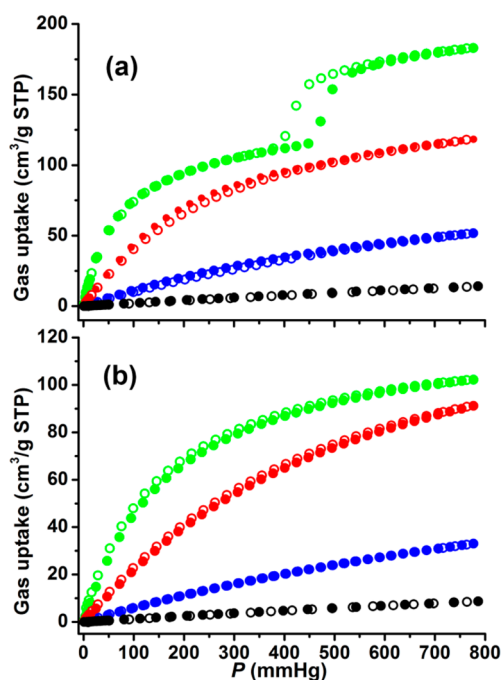


Figure 4. C₂H₂, CO₂, CH₄, and N₂ sorption isotherms (a) at 273 K and (b) at 296 K (C₂H₂: green, CO₂: red, CH₄: blue, N₂: black, solid symbols: adsorption, open symbols: desorption).

cm³), which is not only the highest among all HOFs so far, but also comparable to those few MOFs with high acetylene storage capacities.²¹

CO₂ uptakes of HOF-5a at 273 and 296 K (1 atm) are 117.1 cm³/g (111.8 cm³/cm³) and 90.0 cm³/g (86.0 cm³/cm³), respectively, demonstrating HOF-5a as the best HOF material for potential carbon dioxide capture and separation. Its carbon dioxide capture capacities are even comparable to one of the best MOFs, HKUST-1 Cu₃(BTC)₂.²² As expected, HOF-5a (under 1 atm) takes up much less methane 50.9 cm³/g at 273 K; 32.0 cm³/g at 296 K and nitrogen 13.4 cm³/g at 273 K; 8.2 cm³/g at 296 K under 1 atm.

The coverage-dependent adsorption enthalpies of HOF-5a to C₂H₂, CO₂, C₂H₄, and N₂ were calculated using their adsorption isotherms at 273 and 296 K according to the virial method (Figure S11). The enthalpies at zero coverage are 27.6, 22.8, 19.2, and 14.1 kJ/mol for C₂H₂, CO₂, CH₄, and N₂,

respectively, which confirms the gas affinity in the order of C₂H₂ > CO₂ > CH₄ > N₂.

We further examined the potential of HOF-5a for gas separations. The mixture selectivities at different pressures and temperatures were calculated based on the well-known ideal adsorbed solution theory (IAST) for mixed C₂H₂/CH₄ (50:50), CO₂/CH₄ (50:50), and CO₂/N₂ (10:90) (Figures 5

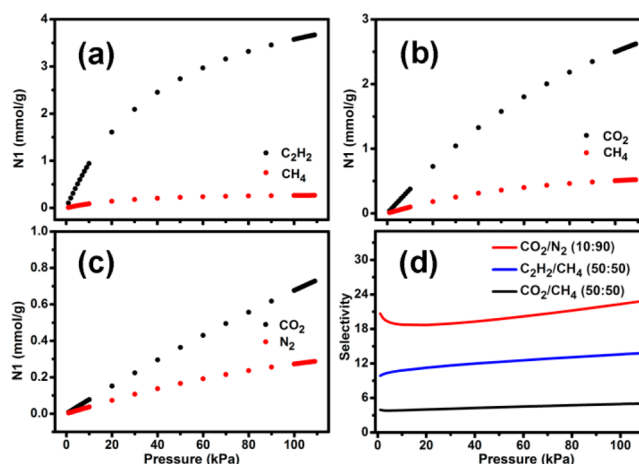


Figure 5. Mixture adsorption isotherms (a–c) and gas selectivities (d) of HOF-5a at 296 K predicted by IAST for C₂H₂/CH₄ (50:50), CO₂/CH₄ (50:50), and CO₂/N₂ (10:90).

and S12–S14 and Table S2). The C₂H₂/CH₄ and CO₂/CH₄ molar selectivities for HOF-5a have been predicted to be 13.6 and 5.0, respectively, at 296 K and 1 atm. CO₂/N₂ selectivity for a 10:90 mixture, a mimic composition in postcombustion carbon dioxide capture, is 22.4 at 296 K and 1 atm. It needs to be pointed out that HOF-5a not only has the highest CO₂ capture amount among the reported HOFs, but also displays a high CO₂/N₂ selectivity,^{8,9} underlying the uniqueness of this new HOF for carbon dioxide capture and separation.

Binding Sites within HOF-5a for Carbon Dioxide Capture. The CO₂ uptake at 296 K corresponds to ~3.1 mol of CO₂ adsorbed per mole of HOF-5a. To probe the CO₂ preferential adsorption sites, neutron diffraction measurement was performed. The data of HOF-5a loaded with ~1.5CO₂ per organic linker molecule (HOF-5a ⊃ 1.5CO₂) are shown in Figure 6 along with Rietveld structural refinement. Two

Table 3. Comparison of BET Surface Area, Acetylene Uptake, and Carbon Dioxide Uptake in Reported HOFs

HOFs	BET S _A (m ² /g)	C ₂ H ₂ (cm ³ /g)		CO ₂ (cm ³ /g)		framework density (g/cm ³) ^e	ref
		273 K	296 K	273 K	296 K		
Ni(tame) ₂ (PES) ₂	392 ^a	–	–	–	–	–	8a
SOF-1a	474 ^b	61	50	30	16	0.931	8b
HOF-8	–	–	–	–	57	1.133	8c
TTBI	2796 ^a	–	–	81	–	0.755	8d
SOF-7a	900 ^c	–	–	64	33	0.883	8e
TPZ	1159 ^a	–	–	–	–	1.059	8f
HOF-1a	359 ^d	63	55	–	–	0.835	9a
HOF-2a	238 ^d	–	–	–	–	0.883	9b
HOF-3a	165 ^d	58	47	31	21	0.430	9c
HOF-4a	312 ^d	–	–	–	–	0.899	9d
HOF-5a	1101 ^a	182	102	117	90	0.955	this work

^aDetermined from N₂ isotherm at 77 K. ^bCalculated from N₂ adsorption at 125 K. ^cDeduced from CO₂ adsorption at 273 K. ^dDetermined from CO₂ adsorption at 196 K. ^eCalculation based on the crystal data without consideration of solvent molecules.

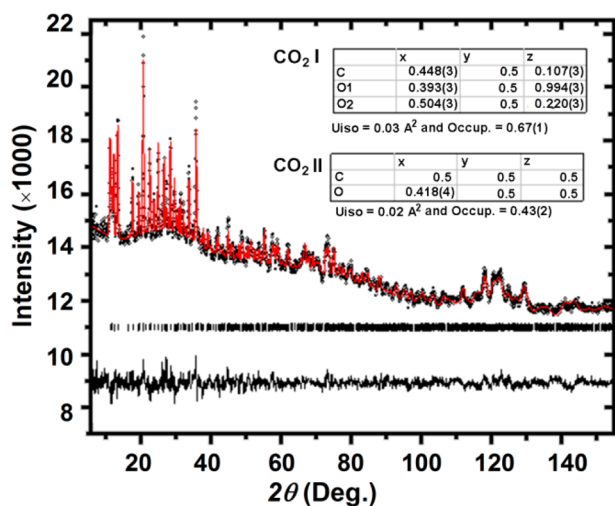


Figure 6. Experimental (circles), calculated (line), and difference (line below observed and calculated patterns) powder neutron diffraction profiles for HOF-5a loaded with CO₂ measured at 200 K. CO₂ molecules were kept as rigid bodies during the Rietveld structural refinement. Vertical bars indicate the calculated positions of Bragg peaks. Goodness of fit data: $R_{wp} = 0.0123$, $R_p = 0.0093$, $\chi^2 = 1.42$. The refined gas molecule coordinates are shown in the inset.

primary CO₂ adsorption sites were identified from the data. The refined CO₂ concentration is $\sim 1.44\text{CO}_2$ per organic linker molecule, consistent with the experimental amount of gas ($\sim 1.5\text{CO}_2$ per L molecule) loaded into the material. Figure 7a and b show the preferential CO₂ binding positions (sites I and II) and orientations. The CO₂ molecules are located on these sites filling in the cavities along the [001] direction. Full occupancy of the two CO₂ sites identified from neutron diffraction (3 mol of CO₂ per mol of HOF-5a) would largely account for the CO₂ uptake at 296 K and 1 atm (~ 3.1 mol of CO₂ per mol of HOF-5a) as observed in the adsorption isotherm.

To evaluate the CO₂ adsorption energetics in HOF-5a, we performed dispersion-corrected density functional theory (DFT-D) calculations.^{19,20} The DFT-D optimized CO₂ adsorption configurations (see Table S3) are in excellent agreement with the experimental results, strongly corroborating our structural analysis of the neutron diffraction data. The calculated static CO₂ binding energies are 39.9 and 37.3 kJ/mol for the two respective CO₂ adsorption sites. This small difference in binding energies on these two energetically favored sites is in line with the fact that these two sites get populated simultaneously with different occupancies as indicated in the diffraction data.

In the present case, the expected strong hydrogen bonds between the CO₂ molecules and DAT moieties were not observed since all amino groups were utilized to support the hydrogen-bonded organic channels of HOF-5a. The carbon dioxide interactions with the hydrogen-bonded organic framework are mainly of van der Waals nature. The moderately strong host-guest interaction is indicated by the nearest distance of 3.36 Å between the C atom of carbon dioxide (site I) and the N atom in HOF-5a (Figure 7a).²³ For site II, the CO₂ molecule interacts with HOF-5a via the C-H...O interaction, as implied by the short H...O distance of 2.80 Å. In addition, two kinds of weak interactions between neighboring carbon dioxide molecules are suggested in terms of the short C...O separation of 3.45 Å for adjacent carbon

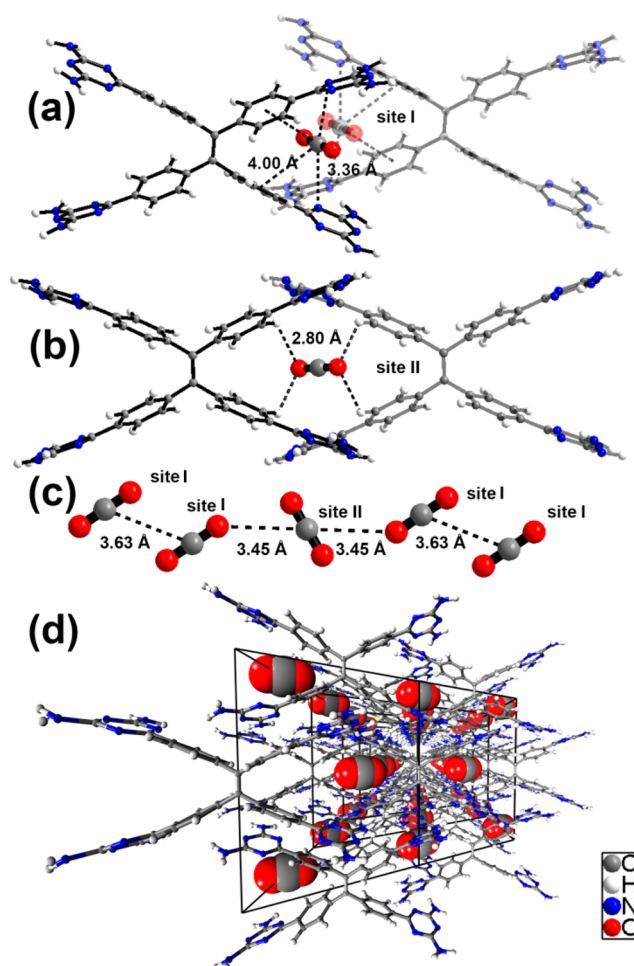


Figure 7. Neutron diffraction crystal structure of HOF-5a $\supset 1.5\text{CO}_2$ showing (a and b) preferential binding sites for CO₂ uptake (sites I and II) and their close contacts with the framework fragments; (c) weak interactions among CO₂ molecules located at binding sites I and II to form a pseudo-one-dimensional array; (d) packing diagram illustrating the high density of adsorbed CO₂ molecules.

dioxide molecules (one on site I and the other on site II) as well as the C...C separation of 3.63 Å between adjacent CO₂ (both on site I), which links those CO₂ molecules into pseudo-one-dimensional arrays (Figure 7b and 7c) along the [001] direction, and largely contributes to the high density of adsorbed CO₂ molecules in HOF-5a. The unique pore structure with suitable pore sizes, curvatures, and functional sites has enabled HOF-5a to take up a large amount of CO₂ molecules.

CONCLUSIONS

In summary, we have realized the first example of a highly porous (robust) and flexible hydrogen-bonded organic framework (HOF-5), exhibiting a significant framework contraction of $\sim 21\%$ with respect to the activated species. Compared with those developed HOFs with less porosities before,⁹ not only does this HOF have multiple DAT moieties, but also more importantly, these DAT moieties are oriented in a way to enforce a large number of strong hydrogen bonding interactions (each organic linker in HOF-5a is linked by eight organic linkers but via 24 hydrogen bonds between DATs), thus stabilizing the framework. The suitable pore sizes, curvatures, and functional sites on the pore surfaces enable

this HOF to take up a large amount of carbon dioxide molecules (the highest carbon dioxide uptake among reported HOFs), which has been revealed in the sorption isotherms, neutron powder diffraction studies, and theoretical calculations. This work not only demonstrates the uniqueness of HOFs, but also establishes some common features between MOFs and HOFs. We hope that these findings stimulate more extensive research on HOFs in both the chemistry and materials science communities.

■ ASSOCIATED CONTENT

■ Supporting Information

Supramolecular structures of HOF-5 and HOF-5a, photographs of as-synthesized HOF-5 and HOF-5a, powder XRD patterns of HOF-5 and HOF-5a, TGA curve of HOF-5, mixture adsorption isotherms and selectivities of CO₂/CH₄ (50:50) and CO₂/N₂ (10:90) predicted by IAST at 273 K. (PDF). X-ray crystallographic data for HOF-5. (CIF). X-ray crystallographic data for HOF-5a. (CIF). The Supporting Information is available free of charge on the ACS Publications website at DOI: 10.1021/jacs.5b05644.

■ AUTHOR INFORMATION

Corresponding Authors

*wzhou@nist.gov

*banglin.chen@utsa.edu

Notes

The authors declare no competing financial interest.

■ ACKNOWLEDGMENTS

This work was supported by the grant AX-1730 from the Welch Foundation (B.C.).

■ REFERENCES

- (1) (a) Yu, J.; Xu, R. *Acc. Chem. Res.* **2010**, *43*, 1195. (b) Linares, N.; Silvestre-Albero, A. M.; Serrano, E.; Silvestre-Albero, J.; Garcia-Martinez, J. *Chem. Soc. Rev.* **2014**, *43*, 7681. (c) Roth, W. J.; Nachtigall, P.; Morris, R. E.; Čejka, J. *Chem. Rev.* **2014**, *114*, 4807.
- (2) (a) Zhao, D.; Feng, J.; Huo, Q.; Melosh, N.; Frederickson, G. H.; Chmelka, B. F.; Stucky, G. D. *Science* **1998**, *279*, 548. (b) Davis, M. E. *Acc. Chem. Res.* **1993**, *26*, 111. (c) Valtchev, V.; Tosheva, L. *Chem. Rev.* **2013**, *113*, 6734. (d) Navalon, S.; Dhakshinamoorthy, A.; Alvaro, M.; Garcia, H. *Chem. Rev.* **2014**, *114*, 6179. (e) Yue, Y.; Mayes, R. T.; Kim, J.; Fulvio, P. F.; Sun, X.-G.; Tsouris, C.; Chen, J.; Brown, S.; Dai, S. *Angew. Chem., Int. Ed.* **2013**, *52*, 13458.
- (3) (a) Furukawa, H.; Cordova, K. E.; O'Keeffe, M.; Yaghi, O. M. *Science* **2013**, *341*, 974. (b) Zhang, J.-P.; Zhang, Y.-B.; Lin, J.-B.; Chen, X.-M. *Chem. Rev.* **2012**, *112*, 1001. (c) Sato, H.; Kosaka, W.; Matsuda, R.; Hori, A.; Hijikata, Y.; Belosludov, R. V.; Sakaki, S.; Takata, M.; Kitagawa, S. *Science* **2014**, *343*, 167. (d) Li, J.-R.; Sculley, J.; Zhou, H.-C. *Chem. Rev.* **2012**, *112*, 869. (e) Zhu, Q.-L.; Xu, Q. *Chem. Soc. Rev.* **2014**, *43*, 5468. (f) Eddaoudi, M.; Sava, D. F.; Eubank, J. F.; Adil, K.; Guillermin, V. *Chem. Soc. Rev.* **2015**, *44*, 228. (g) Cui, Y.; Yue, Y.; Qian, G.; Chen, B. *Chem. Rev.* **2012**, *112*, 1126. (h) Chen, B.; Xiang, S.; Qian, G. *Acc. Chem. Res.* **2010**, *43*, 1115. (i) Zhao, X.; Bu, X.; Zhai, Q.-G.; Tran, H.; Feng, P. *J. Am. Chem. Soc.* **2015**, *137*, 1396.
- (4) (a) Vaidyanathan, R.; Iremonger, S. S.; Shimizu, G. K. H.; Boyd, P. G.; Alavi, S.; Woo, T. K. *Science* **2010**, *330*, 650. (b) Serre, C.; Mellot-Drazniak, C.; Surblé, S.; Audebrand, N.; Filinchuk, Y.; Férey, G. *Science* **2007**, *315*, 1828. (c) Zhang, Z.; Zaworotko, M. J. *Chem. Soc. Rev.* **2014**, *43*, 5444. (d) Wu, H.; Gong, Q.; Olson, D. H.; Li, J. *Chem. Rev.* **2012**, *112*, 836. (e) Gao, W.-Y.; Chrzanowski, M.; Ma, S. *Chem. Soc. Rev.* **2014**, *43*, 5841. (f) Li, T.; Kozłowski, M. T.; Doud, E. A.; Blakely, M. N.; Rosi, N. L. *J. Am. Chem. Soc.* **2013**, *135*, 11688. (g) Chen, L.; Reiss, P. S.; Chong, S. Y.; Holden, D.; Jelfs, K. E.; Hasell,

- T.; Little, M. A.; Kewley, A.; Briggs, M. E.; Stephenson, A.; Thomas, K. M.; Armstrong, J. A.; Bell, J.; Busto, J.; Noel, R.; Liu, J.; Strachan, D. M.; Thallapally, P. K.; Cooper, A. I. *Nat. Mater.* **2014**, *13*, 954. (h) Wang, C.; Zhang, T.; Lin, W. *Chem. Rev.* **2012**, *112*, 1084. (i) Farha, O. K.; Yazaydin, O.; Eryazici, I.; Malliakas, C.; Hauser, B.; Kanatzidis, M. G.; Nguyen, S. T.; Snurr, R. Q.; Hupp, J. T. *Nat. Chem.* **2010**, *2*, 944. (j) Wang, Z.; Cohen, S. M. *Chem. Soc. Rev.* **2009**, *38*, 1315. (k) Wu, H.; Chua, Y. S.; Krungleviciute, V.; Tyagi, M.; Chen, P.; Yildirim, T.; Zhou, W. *J. Am. Chem. Soc.* **2013**, *135*, 10525.
- (5) (a) Doonan, C. J.; Tranchemontagne, D. J.; Glover, T. G.; Hunt, J. R.; Yaghi, O. M. *Nat. Chem.* **2010**, *2*, 235. (b) Xu, Y.-H.; Jin, S.-B.; Xu, H.; Nagai, A.; Jiang, D.-L. *Chem. Soc. Rev.* **2013**, *42*, 8012.
- (6) (a) Wuest, J. D. *Chem. Commun.* **2005**, 5830. (b) Simard, M.; Wuest, J. D. *J. Am. Chem. Soc.* **1991**, *113*, 4696. (c) Tian, J.; Thallapally, P. K.; McGrail, B. P. *CrystEngComm* **2012**, *14*, 1909. (d) McKeown, N. B. *J. Mater. Chem.* **2010**, *20*, 10588. (e) Kolotuchin, S. V.; Fenlon, E. E.; Wilson, S. R.; Loweth, C. J.; Zimmerman, S. C. *Angew. Chem., Int. Ed. Engl.* **1995**, *34*, 2654.
- (7) (a) Endo, K.; Sawaki, T.; Koyanagi, M.; Kobayashi, K.; Masuda, H.; Aoyama, Y. *J. Am. Chem. Soc.* **1995**, *117*, 8341. (b) Brunet, P.; Simard, M.; Wuest, J. D. *J. Am. Chem. Soc.* **1997**, *119*, 2737. (c) Holman, K. T.; Pivovar, A. M.; Swift, J. A.; Ward, M. D. *Acc. Chem. Res.* **2001**, *34*, 107. (d) Saied, O.; Maris, T.; Wuest, J. D. *J. Am. Chem. Soc.* **2003**, *125*, 14956. (e) Kobayashi, K.; Sato, A.; Sakamoto, S.; Yamaguchi, K. *J. Am. Chem. Soc.* **2003**, *125*, 3035. (f) Malek, N.; Maris, T.; Perron, M.; Wuest, J. D. *Angew. Chem., Int. Ed.* **2005**, *44*, 4021. (g) Maly, K. E.; Gagnon, E.; Maris, T.; Wuest, J. D. *J. Am. Chem. Soc.* **2007**, *129*, 4306. (h) Liu, Y.; Hu, C.; Comotti, A.; Ward, M. D. *Science* **2011**, *333*, 436. (i) Yamamoto, A.; Hamada, T.; Hisaki, I.; Miyata, M.; Tohna, N. *Angew. Chem., Int. Ed.* **2013**, *52*, 1709. (j) Xiao, W.; Hu, C.; Ward, M. D. *J. Am. Chem. Soc.* **2014**, *136*, 14200. (k) Reddy, D. S.; Duan, S.; Shimizu, G. K. H. *Angew. Chem., Int. Ed.* **2003**, *42*, 1360. (l) Görbitz, C. H. *Chem. - Eur. J.* **2001**, *7*, 5153. (m) Görbitz, C. H. *Chem. - Eur. J.* **2007**, *13*, 1022. (n) Soldatov, D. V.; Moudrakovski, I. L.; Grachev, E. V.; Ripmeester, J. A. *J. Am. Chem. Soc.* **2006**, *128*, 6737. (o) Natarajan, R.; Magro, G.; Bridgland, L. N.; Sirikulkajorn, A.; Narayanan, S.; Ryan, L. E.; Haddow, M. F.; Orpen, A. G.; Charmant, J. P. H.; Hudson, A. J.; Davis, A. P. *Angew. Chem., Int. Ed.* **2011**, *50*, 11386.
- (8) (a) Dalrymple, S. A.; Shimizu, G. K. H. *J. Am. Chem. Soc.* **2007**, *129*, 12114. (b) Yang, W.; Greenaway, A.; Lin, X.; Matsuda, R.; Blake, A. J.; Wilson, C.; Lewis, W.; Hubberstey, P.; Kitagawa, S.; Champness, N. R.; Schröder, M. *J. Am. Chem. Soc.* **2010**, *132*, 14457. (c) Luo, X.-Z.; Jia, X.-J.; Deng, J.-H.; Zhong, J.-L.; Liu, H.-J.; Wang, K.-J.; Zhong, D.-C. *J. Am. Chem. Soc.* **2013**, *135*, 11684. (d) Mastalerz, M.; Oppel, I. M. *Angew. Chem., Int. Ed.* **2012**, *51*, 5252. (e) Lü, J.; Perez-Krap, C.; Suyetin, M.; Alsmail, N. H.; Yan, Y.; Yang, S.; Lewis, W.; Bichoutskaia, E.; Tang, C. C.; Blake, A. J.; Cao, R.; Schröder, M. *J. Am. Chem. Soc.* **2014**, *136*, 12828. (f) Chen, T.-H.; Popov, I.; Kaveevivitchai, W.; Chuang, Y.-C.; Chen, Y.-S.; Daugulis, O.; Jacobson, A. J.; Miljanić, O. Š. *Nat. Commun.* **2014**, *5*, 5131. (g) Dalapati, S.; Saha, R.; Jana, S.; Patra, A. K.; Bhaumik, A.; Kumar, S.; Guichhait, N. *Angew. Chem., Int. Ed.* **2012**, *51*, 12534. (h) Hisaki, I.; Nakagawa, S.; Tohnai, N.; Miyata, M. *Angew. Chem., Int. Ed.* **2015**, *54*, 3008. (i) Natarajan, R.; Bridgland, L.; Sirikulkajorn, A.; Lee, J.-H.; Haddow, M. F.; Magro, G.; Ali, B.; Narayanan, S.; Strickland, P.; Charmant, J. P. H.; Orpen, A. G.; McKeown, N. B.; Bezzu, C. G.; Davis, A. P. *J. Am. Chem. Soc.* **2013**, *135*, 16912. (j) Soldatov, D. V.; Moudrakovski, I. L.; Ripmeester, J. A. *Angew. Chem., Int. Ed.* **2004**, *43*, 6308. (k) Thallapally, P. K.; McGrail, B. P.; Atwood, J. L.; Gaeta, C.; Tedesco, C.; Neri, P. *Chem. Mater.* **2007**, *19*, 3354. (l) Tian, J.; Thallapally, P. K.; Dalgarno, S. J.; Atwood, J. L. *J. Am. Chem. Soc.* **2009**, *131*, 13216. (m) Afonso, R. V.; Durão, J.; Mendes, A.; Damas, A. M.; Gales, L. *Angew. Chem., Int. Ed.* **2010**, *49*, 3034.
- (9) (a) He, Y.; Xiang, S.; Chen, B. *J. Am. Chem. Soc.* **2011**, *133*, 14570. (b) Li, P.; He, Y.; Zhao, Y.; Weng, L.; Wang, H.; Krishna, R.; Wu, H.; Zhou, W.; O'Keeffe, M.; Han, Y.; Chen, B. *Angew. Chem., Int. Ed.* **2015**, *54*, 574. (c) Li, P.; He, Y.; Arman, H. D.; Krishna, R.; Wang, H.; Weng, L.; Chen, B. *Chem. Commun.* **2014**, *50*, 13081. (d) Li, P.;

He, Y.; Guang, J.; Weng, L.; Zhao, J. C.-G.; Xiang, S.; Chen, B. *J. Am. Chem. Soc.* **2014**, *136*, 547. (e) Yang, W.; Li, B.; Wang, H.; Alduhaish, O.; Alfooty, K.; Aldin Zayed, M.; Li, P.; Arman, H. D.; Chen, B. *Cryst. Growth Des.* **2015**, *15*, 2000.

(10) Li, R.; Hu, W.; Liu, Y.; Zhu, D. *Acc. Chem. Res.* **2010**, *43*, 529.

(11) Buckles, R. E.; Hausman, E. A.; Wheeler, N. G. *J. Am. Chem. Soc.* **1950**, *72*, 2494.

(12) Bhunia, A.; Vasylyeva, V.; Janiak, C. *Chem. Commun.* **2013**, *49*, 3961.

(13) Sun, Z.; Li, Y.; Chen, L.; Jing, X.; Xie, Z. *Cryst. Growth Des.* **2015**, *15*, 542.

(14) Myers, A. L.; Prausnitz, J. M. *AIChE J.* **1965**, *11*, 121.

(15) Li, B.; Zhang, Y.; Krishna, R.; Yao, K.; Han, Y.; Wu, Z.; Ma, D.; Shi, Z.; Pham, T.; Space, B.; Liu, J.; Thallapally, P. K.; Liu, J.; Chrzanowski, M.; Ma, S. *J. Am. Chem. Soc.* **2014**, *136*, 8654.

(16) Sheldrick, G. M. *Acta Crystallogr., Sect. A: Found. Crystallogr.* **2008**, *A64*, 112.

(17) Spek, A. L. *PLATON, A Multipurpose Crystallographic Tool*; Utrecht University: Utrecht, the Netherlands, 2005.

(18) Larson, A. C.; Von Dreele, R. B. *General Structure Analysis System*, Report LAUR 86-748; Los Alamos National Laboratory: Los Alamos, NM, 1994.

(19) Giannozzi, P.; Baroni, S.; Bonini, N.; Calandra, M.; Car, R.; Cavazzoni, C.; Ceresoli, D.; Chiarotti, G. L.; Cococcioni, M.; Dabo, I.; Dal Corso, A.; Fabris, S.; Fratesi, G.; de Gironcoli, S.; Gebauer, R.; Gerstmann, U.; Gougoussis, C.; Kokalj, A.; Lazzeri, M.; Martin-Samos, L.; Marzari, N.; Mauri, F.; Mazzarello, R.; Paolini, S.; Pasquarello, A.; Paulatto, L.; Sbraccia, C.; Scandolo, S.; Sclauzero, G.; Seitsonen, A. P.; Smogunov, A.; Umari, P.; Wentzcovitch, R. M. *J. Phys.: Condens. Matter* **2009**, *21*, 395502.

(20) Barone, V.; Casarin, M.; Forrer, D.; Pavone, M.; Sambri, M.; Vittadini, A. *J. Comput. Chem.* **2009**, *30*, 934.

(21) (a) Xiang, S.; Zhou, W.; Gallegos, J. M.; Liu, Y.; Chen, B. *J. Am. Chem. Soc.* **2009**, *131*, 12415. (b) He, Y.; Krishna, R.; Chen, B. *Energy Environ. Sci.* **2012**, *5*, 9107.

(22) (a) Sumida, K.; Rogow, D. L.; Mason, J. A.; McDonald, T. M.; Bloch, E. D.; Herm, Z. R.; Bae, T.-H.; Long, J. R. *Chem. Rev.* **2012**, *112*, 724. (b) Zhang, Z.; Yao, Z.-Z.; Xiang, S.; Chen, B. *Energy Environ. Sci.* **2014**, *7*, 2868.

(23) Liao, P.-Q.; Zhou, D.-D.; Zhu, A.-X.; Jiang, L.; Lin, R.-B.; Zhang, J.-P.; Chen, X.-M. *J. Am. Chem. Soc.* **2012**, *134*, 17380.